

Hydroformylation and Isomerization of Allene and Propyne: A Density Functional Theory Study

Chun-Fang Huo,^[a] Yong-Wang Li,^[a] Matthias Beller,^[b] and Haijun Jiao*^[a, b]

Dedicated to Professor Paul von Ragué Schleyer on the occasion of his 75th birthday

Abstract: The $[\text{HCo}(\text{CO})_3]$ -catalyzed hydroformylation of allene and propyne has been investigated at the B3LYP level of density functional theory. It is found that hydroformylation of allene favors the linear anti-Markovnikov product in high regioselectivity both kinetically and thermodynamically. The origin of this regioselectivity comes from the enhanced stability of the η^3 -allylic intermediate $[(\eta^3\text{-CH}_2\text{CHCH}_2)\text{Co}(\text{CO})_3]$. By contrast, propyne does not show any regioselectivity. The possible interconversion between allene and propyne mediated by $[\text{HCo}(\text{CO})_3]$ has been explored.

Keywords: allenes • density functional calculations • hydroformylation • propyne • regioselectivity

Introduction

Hydroformylation (“oxo synthesis”) of olefins to give aldehydes as predominant products, discovered by Roelen in 1938, is an intriguing and well-studied reaction.^[1–7] Today, this method has developed into an extremely important industrial process with worldwide capacity over six million tons per year.^[4] Surprisingly, the product range of technical hydroformylation has remained nearly unchanged in the past five decades, although during the stage of 1965 to 1980 a remarkable diversification of products, refinement of methods and further development of the Co-based processes took place as did the initial penetration and substitution of these processes by Rh-based catalysts.^[8] Up until now, the expansion of the products by modifying catalysts and utiliz-


ing the diverse feedstock is still a challenging and promising project.

The hydroformylation of alkynes and allenes is a potential route for producing α,β -unsaturated aldehydes, which are valuable intermediates in fine chemicals and pharmacy. Since the Co-catalyzed acetylene hydroformylation first reported by Natta and Pino^[9] in 1951, increasing attention^[10–20] has been devoted to this field. The early studies^[10–16] found that alkynes hydroformylation usually suffered from the low selectivity and/or low yield of unsaturated aldehydes. Fortunately, during the latest two decades, several effective catalysts such as the catalyst system of $[\text{Rh}(\text{CO})_2(\text{acac})]$ and a sophisticated bisphosphite ligand,^[17] the heterobimetallic catalyst $[\text{PdCl}_2(\text{PCy}_3)_2]/[\text{Co}_2(\text{CO})_8]$,^[18] and the zwitterionic rhodium complex with triphenyl phosphite as ligand^[19,20] were developed. These exciting achievements revealed that the hydroformylation of acetylenic species to α,β -unsaturated aldehydes with high activity and selectivity is accessible.

Due to the presence of the cumulated diene structural unit, allenes exhibit some unique reaction behaviors and serve as potential precursors in the synthesis of highly complex and strained target molecules of biological and industrial importance.^[21] Therefore, the chemistry of allenes has attracted much attention of chemists. For example, acylboration,^[22] annulation,^[23] addition of pronucleophiles,^[24] carbonylation,^[25] hydroamination,^[26] and insertion reaction^[27] have been studied extensively. However, the information about the allenes hydroformylation is relatively scant. One experimental study was carried out by Fell and Beutler in 1976,^[28]

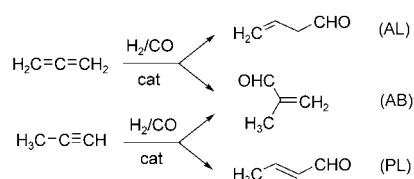
[a] Dr. C.-F. Huo, Dr. Y.-W. Li, Dr. H. Jiao
The State Key Laboratory of Coal Conversion
Institute of Coal Chemistry, Chinese Academy of Sciences
Taiyuan 030001 (PR China)

[b] Prof. Dr. M. Beller, Dr. H. Jiao
Leibniz-Institut für Organische Katalyse
an der Universität Rostock e.V.
Buchbinderstrasse 5–6, 18055 Rostock (Germany)
Fax: (+49) 381-466-9324
E-mail: hjiao@ifok.uni-rostock.de

 Supporting information for this article is available on the WWW under <http://www.chemeurj.org/> or from the author: Total electronic energies, zero-point energies (ZPE), thermal correction to enthalpies and Gibbs free energies, and the optimized Cartesian coordinates for all systems are listed.

and they found that hydroformylation of 1,2-dienes gave mixtures of mono- and dialdehydes. Nevertheless, no theoretical studies have been reported so far.

For terminal alkynes instead of acetylene as substrates, the alkynes insertion into the Co–H bond can occur in two ways, for example, anti-Markovnikov for linear isomers and Markovnikov for branched isomers (Scheme 1).^[29] The same can also be found for allenes. In addition, it is possible for mutual isomerization between alkynes and allenes. This may also result in the diversification of products. Therefore, the key problem of 1,2-dienes or terminal alkynes hydroformylation is how to get the expected α,β -unsaturated aldehyde products, that is to say, how to adjust the regioselectivity to meet with the actual demands.



Scheme 1. Hydroformylation of allene and propyne.

In our previous work,^[30] the detailed mechanism of the $[\text{HCo}(\text{CO})_3]$ -catalyzed acetylene hydroformylation has been explored by using the B3LYP density functional method, and a characteristic catalytic cycle similar to the Heck–Breslow mechanism^[31] for olefin hydroformylation is found. The present theoretical study is aimed at clarifying the regioselectivity of $[\text{HCo}(\text{CO})_3]$ -catalyzed hydroformylation of allene and propyne. The entire catalytic cycles of allene/propyne hydroformylation are investigated with the B3LYP density functional method, and three elementary steps, that is, allene/propyne coordination, allene/propyne insertion, and CO addition, are emphasized. Particularly, the detailed mechanism of the catalytic isomerization of propyne and allene is proposed and discussed. Based on these results, the product distribution is predicted, and the origin of the regioselectivity is elucidated.

Computational Details

All calculations were performed at the B3LYP/6-311+G(d) density functional level of theory as implemented in the Gaussian 03 program.^[32] The geometries of the intermediates and the transition states were fully optimized without any symmetry constraints, if not noted otherwise. The frequencies were analyzed at the same level to confirm the optimized structures to be ground states without imaginary frequency ($\text{NImag}=0$) or transition states (TS) with one imaginary frequency ($\text{NImag}=1$). Especially, the lone imaginary frequency of each transition state displayed the desired displacements orientation, and the validity of each reaction path was further examined by the intrinsic reaction coordinate (IRC) calculations. In addition, the enthalpies and the Gibbs free energies^[33] were calculated at actual reaction conditions of 403.15 K and 200 atm. Considering the entropy effects, the following discussions are based on the free energies (ΔG) of activation and reaction, and the corresponding enthalpies (ΔH) are provided in square bracket in energy profiles for compari-

son. The calculated total electronic energies, ZPE and thermal corrections to enthalpies and Gibbs free energies are available in the Supporting Information.

Results and Discussion

As shown in Scheme 1, allene and propyne insertion into the Co–H bond lead to the different anti-Markovnikov products, although they share the same Markovnikov intermediate. In this section, the $[\text{HCo}(\text{CO})_3]$ -catalyzed allene/propyne coordination and insertion are thoroughly investigated at first. Next, the following steps, CO addition and insertion, H_2 oxidative addition and unsaturated aldehyde elimination, are briefly discussed along three paths for yielding $\text{H}_2\text{C}=\text{CHCH}_2\text{CHO}$ (AL), $\text{H}_2\text{C}=\text{C}(\text{CH}_3)\text{CHO}$ (AB) and $\text{H}_3\text{CHC}=\text{CHCHO}$ (PL), respectively. After that, two possible reaction pathways for the catalytic isomerization of propyne and allene are proposed and explored in detail. Finally, the influence of the isomerization on the product selectivity of the hydroformylation is analyzed, and the origin of the regioselectivity is revealed.

Allene coordination and insertion: Based on the structural comparability of allene and propene, one can assume that allene should have the similar mechanistic aspect as propene in hydroformylation.^[34] However, the cumulated double bonds of allene may exhibit some unique reaction behaviors. In this section, we focus our discussions on these characteristics. The free energy profiles for allene coordination and insertion steps are shown in Figure 1, whereas the corresponding structures are depicted in Figure 2.

As reported previously,^[35] the formation of $[\text{HCo}(\text{CO})_3]$ via the dissociation of the equatorial CO ligand is more favored than the axial alternative by $10.6 \text{ kcal mol}^{-1}$. The $[\text{HCo}(\text{CO})_3]$ formed in C_{2v} symmetry represents the most stable singlet state, while other structural and electronic isomers are higher in energy.

As shown in Figure 2, there are three π -coordination forms of allene with the planar $[\text{HCo}(\text{CO})_3]$. One has the C=C bond in the equatorial plane (**A1**), and the others have the C=C bond parallel to the Co–H bond, while differ in the $=\text{CH}_2$ direction (**A1-syn** and **A1-anti**, in which *syn* and *anti* mean the orientation of the $=\text{CH}_2$ group to the Co–H bond). On the potential energy surface, **A1** is an energy minimum structure, while **A1-anti** is a transition state for the rotation of the coordinated allene and optimization without symmetry constraint leads to **A1**. The computed allene rotation barrier is $7.7 \text{ kcal mol}^{-1}$. These conclusions differ from those for the propene coordination to $[\text{HCo}(\text{CO})_3]$,^[34] in which all initially constructed conformations are found to be energy minimum structures.

Interestingly **A1-syn** also does not correspond to an energy minimum structure, and structure optimization from **A1-syn** converges to **A1-trans**, in which both Co–H and allene ligand are at the axial sites and three CO ligands are at the equatorial sites. This *trans* arrangement of Co–H and

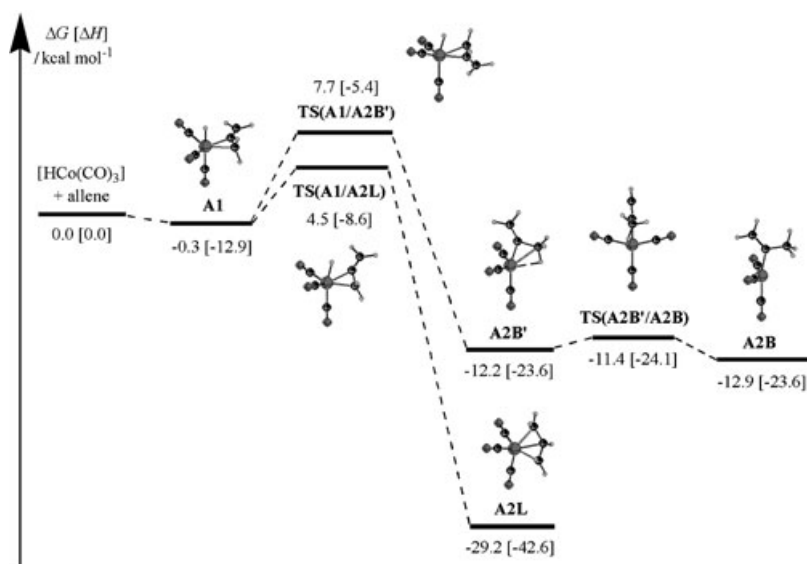


Figure 1. Free energy profiles (kcal mol^{-1} , enthalpies in square brackets) for allene coordination and insertion (relative to $[\text{HCo}(\text{CO})_3] + \text{allene}$).

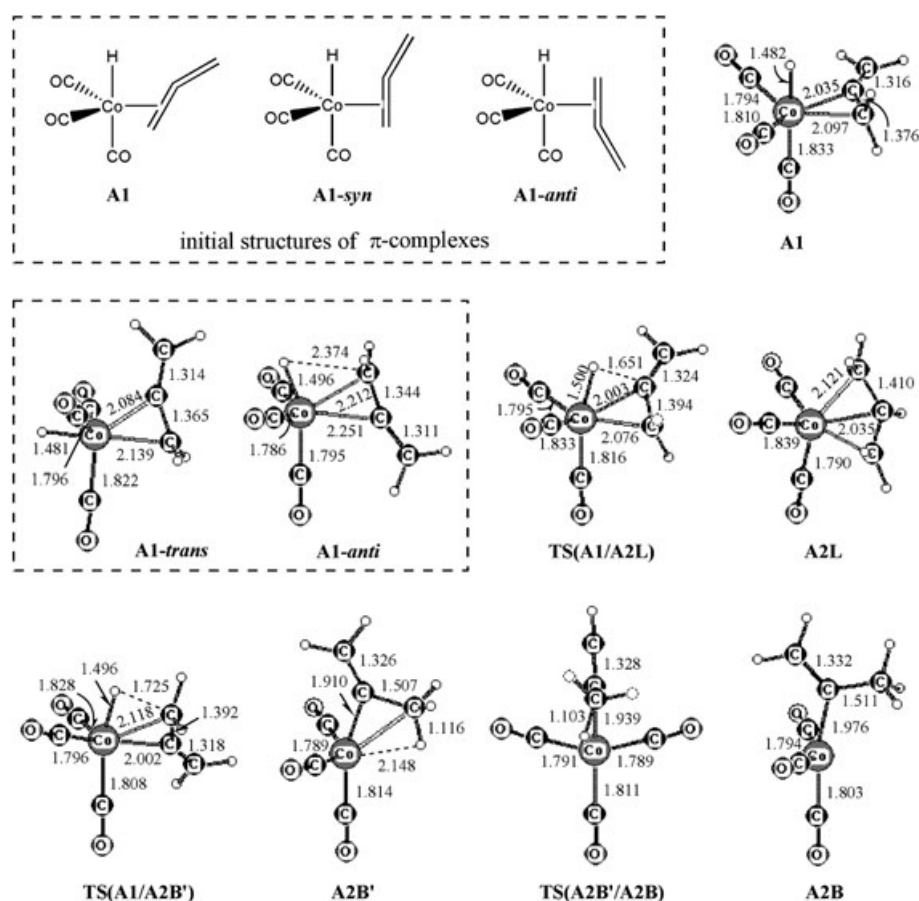


Figure 2. Bond lengths [\AA] of the stationary points involved in allene coordination and insertion.

allene in **A1-trans** does not facilitate the subsequent reaction of allene insertion into the Co–H bond. In addition, the isomer **A1-trans** is higher in free energy than **A1** by $2.6 \text{ kcal mol}^{-1}$. Thus, **A1** represents the most stable form of

allene coordination, and facilitates the subsequent reaction of allene insertion into the Co–H bond. Additionally, the formation of **A1** is slightly exergonic by $0.3 \text{ kcal mol}^{-1}$, and highly exothermic by $12.9 \text{ kcal mol}^{-1}$.

Starting with **A1**, allene insertion into the Co–H bond takes place in two ways, anti-Markovnikov and Markovnikov. This process proceeds by the hydride attacking and transferring to the internal or terminal carbon atom of allene. In our latest work,^[34] propene insertion into the Co–H bond has been investigated in detail. It was found that propene insertion reaction proceeds by stepping via propene rotation and hydride migration leading to the agostic stabilized intermediates, and is a thermally neutral and reversible process. Due to the cumulated double bonds, the insertion behaviors of allene differ strongly from those of propene. As depicted in Figure 1, allene insertion reaction is a one-step process. The anti-Markovnikov and Markovnikov insertion go via the distorted square pyramidal transition states, **TS(A1/A2L)** and **TS(A1/A2B')**, respectively. As compared with **A1**, the characteristic change in **TS(A1/A2L)** and **TS(A1/A2B')** is the approach of the hydride and the allene carbon atom (1.651 and 1.725 Å) coupled with the rotation of the allene moiety (Figure 2). Following the imaginary vibration mode of **TS(A1/A2L)** directing to the insertion product, we have located an anti-Markovnikov intermediate **A2L**; [(CH₂CHCH₂)Co(CO)₃], which has a square pyramidal geometry with a η^3 -coordination of the allylic CH₂CHCH₂ group to [Co(CO)₃] unit instead of a η^1 -propenyl mode. To understand this difference, we are interested in the Co···H–C agostic stabilized conformation of [(CH₂CHCH₂)Co(CO)₃]. The result shows that this agostic species has one imaginary frequency, and is a transition state **TS(A2L/A2L)** for the rotation of the allylic group.

However, for the Markovnikov insertion, two intermediates [(H₂C=CCH₃)Co(CO)₃] have been located. One **A2B'** has a trigonal bipyramidal conformation with the Co···H–C agostic interaction as in the case of (iso)propyl complexes [(C₃H₇)Co(CO)₃],^[34] and the other **A2B** has a tetra-coordinated Co center as in the case of vinyl complex [(H₂C=CH)Co(CO)₃].^[30] **A2B** is slightly more stable than **A2B'** by 0.7 kcal mol^{–1}, and the transformation from **A2B'** to **A2B** needs a small barrier of 0.8 kcal mol^{–1}.

The thermodynamic behavior of allene insertion into the Co–H bond is remarkably different from that of propene. The free energy profiles in Figure 1 clearly show that the insertion of allene into the Co–H bond forming **A2L** and **A2B** is highly exergonic by 28.9 and 12.6 kcal mol^{–1}, and has the free energy barriers of 4.8 and 8.0 kcal mol^{–1}, respectively. These energetic data show that allene insertion reaction is an irreversible process, and thus is responsible for the observed regioselectivity. In addition, the anti-Markovnikov species **TS(A1/A2L)** and **A2L** are lower in free energy than the corresponding Markovnikov species **TS(A1/A2B')** and **A2B** by 3.2 and 16.3 kcal mol^{–1}. It indicates that the formation of **A2L** is more favored both kinetically and thermodynamically, and **A2L** represents the only principal intermediate. The successive consequence is the formation of linear unsaturated aldehyde H₂C=CHCH₂CHO as shown in Scheme 1.

Propyne coordination and insertion: Since allene and propyne have a joint product from the Markovnikov process (Scheme 1), we are interested in the thermodynamic magnitudes of propyne. Because of the detailed analysis of acetylene hydroformylation reported previously,^[30] the main results of propyne hydroformylation are discussed briefly, while the origin of regioselectivity is emphasized. The free energy profiles for propyne coordination and insertion steps are shown in Figure 3, whereas the structures of the stationary points are given in Figure 4.

As expected from acetylene coordination, the most stable propyne π -complex **P1** [HCo(CO)₃(η^2 -HC≡CCH₃)] has the C≡C bond in the equatorial plane. This process is endergonic by 2.4 kcal mol^{–1}, while exothermic by 9.7 kcal mol^{–1}. The other two complexes, **P1-syn** and **P1-anti**, with the C≡C bond parallel to the Co–H bond are transition states for the degenerated enantiomerization of **P1** with free energy barriers of 4.7 and 5.1 kcal mol^{–1}, respectively.

The subsequent propyne insertion into the Co–H bond can occur in two ways leading to the different anti-Markovnikov intermediate **P2L** [(H₃CCH=CH)Co(CO)₃] and the joint Markovnikov intermediate **A2B** [(H₂C=CCH₃)Co(CO)₃], which should also be **P2B** according to our nomenclature. As illustrated in Figure 3, propyne insertion reaction is a one-step and irreversible process, in which the hydride migration is coupled with the skeletal Berry pseudorotation. Furthermore, both insertion pathways are highly exergonic by 16.4 and 15.7 kcal mol^{–1} with the free energy barriers of 7.6 and 7.4 kcal mol^{–1}, respectively. These thermodynamic values are much larger than those of propene hydroformylation.^[34] Interestingly, either two transition states (**TS(P1/P2L)** and **TS(P1/A2B)**) or two intermediates (**P2L** and **A2B**) are very close in energy. **TS(P1/P2L)** is only 0.2 kcal mol^{–1} higher in free energy than **TS(P1/A2B)**, while **P2L** is slightly more stable than **A2B** by 0.7 kcal mol^{–1}. Hence, there is no distinct preference for two insertion paths, and they are not regioselective.

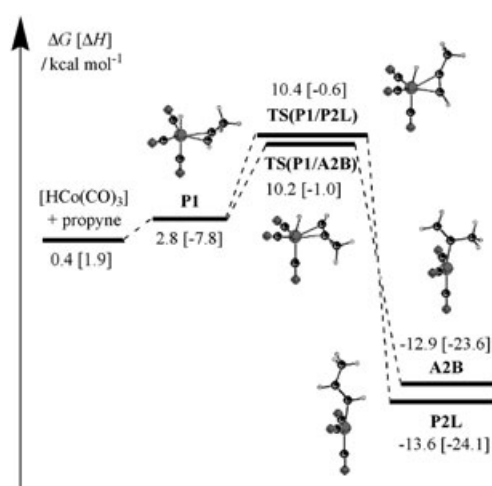


Figure 3. Free energy profiles (kcal mol^{–1}, enthalpies in square brackets) for propyne coordination and insertion (relative to [HCo(CO)₃] + allene).

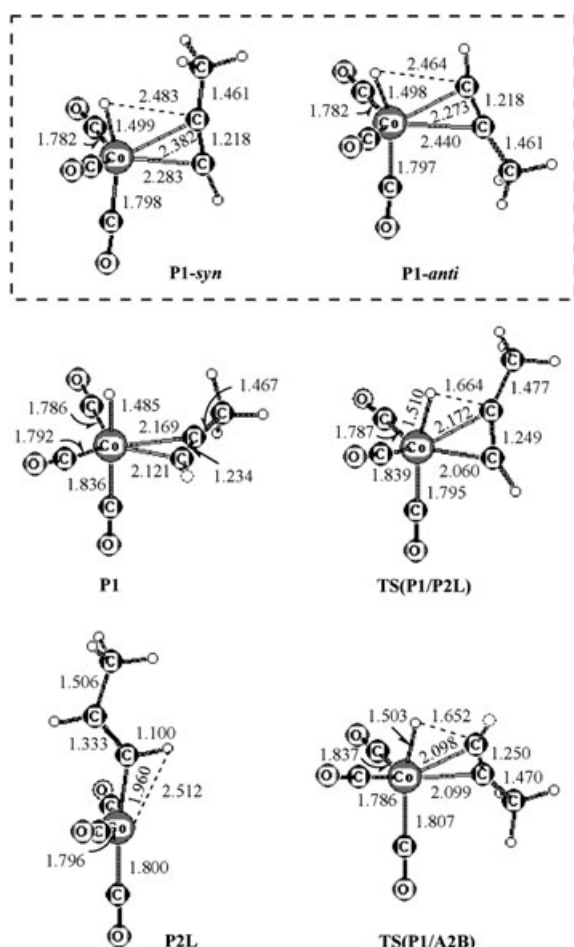


Figure 4. Bond lengths [Å] of the stationary points involved in propyne coordination and insertion.

Formation of unsaturated aldehyde: Following the allene/propyne insertion reaction, the CO addition and insertion, H_2 oxidative addition and unsaturated aldehyde elimination take place in turn along three pathways (AL, AB and PL, Scheme 1) forming unsaturated aldehyde products, $H_2C=CHCH_2CHO$, $H_2C=C(CH_3)CHO$ and $H_3CHC=CHCHO$, respectively. The free energy profiles associated with these processes and the structures of the stationary points are illustrated in Figures 5–10.

As depicted in Figure 5 (top), the CO addition to the η^3 -complex **A2L** forms the trigonal bipyramidal complex **A3L** $[(H_2C=CHCH_2)Co(CO)_4]$. For this step, two transition states have been located. Structures **TS1(A2L/A3L)** and **TS2(A2L/A3L)** represent the CO attack of **A2L** from the front and back sides of the η^3 - H_2CCHCH_2 moiety, respectively (Figure 6). Like **A3L**, both transition states have the trigonal bipyramidal geometries with the allyl group at the axial site, while the incoming CO ligand at the equatorial site. Due to breaking two Co–C bonds, both attacks have the high free energy barriers: 24.6 kcal mol $^{-1}$ for **TS1(A2L/A3L)** and 25.4 kcal mol $^{-1}$ for **TS2(A2L/A3L)**. The close energetic data indicate that two CO attack modes are competi-

tive and possible. Furthermore, the CO addition to **A2L** forming **A3L** is endergonic by 8.8 kcal mol $^{-1}$. This thermodynamic behavior also is opposite to that of propene,^[34] which is highly exergonic process.

From Figure 5 (right side of top, and bottom), we can see that allene hydroformylation yielding linear aldehyde (path AL) has the similar mechanistic aspect as propene^[34] in the processes of CO insertion, H_2 oxidative addition and aldehyde reductive elimination. This similarity is actually expected and therefore, the energetic changes are discussed here, while the structural parameters are presented for comparison. The CO insertion reaction (carbonylation) proceeds via two $[Co(CO)_3]$ pseudorotated transition states (**TS(A3L/A4La)**, **TS(A4La/A4Lb)**) and a Co \cdots H–C agostic stabilized intermediate (**A4La**) leading to the most stable acyl complex $[(H_2C=CHCH_2CO)Co(CO)_3]$ (**A4Lb**), which is stabilized by the equatorial η^2 -O=C interaction. This stepwise process is predicted to be endergonic by 8.2 kcal mol $^{-1}$ and exergonic by 3.6 kcal mol $^{-1}$, with the free energy barriers of 11.5 and 9.6 kcal mol $^{-1}$, respectively. Two H_2 coordination possibilities, **A4Lb** + H_2 \rightarrow **A5La** and **A4La** + H_2 \rightarrow **A5La'**, are competitive and endergonic by 11.2 and 9.4 kcal mol $^{-1}$. The subsequent H_2 oxidative addition (**A5La** \rightarrow **A5La'** \rightarrow **A5Lb**) accomplishes via the acyl group rotation and the H–H dissociation, and the whole process is computed to be endergonic by 4.4 kcal mol $^{-1}$ with small free energy barrier of 5.8 kcal mol $^{-1}$. The final unsaturated aldehyde elimination goes through the three-center transition state **TS(A5Lb/A6L)** forming the adduct **A6L**, which is a rapid and highly exergonic process (–12.6 kcal mol $^{-1}$).

For allene/propyne hydroformylation yielding joint branched aldehyde (path AB, Figure 7) and propyne hydroformylation yielding linear aldehyde (path PL, Figure 9), the cases of CO addition and insertion, H_2 oxidative addition and aldehyde elimination are similar to those of acetylene hydroformylation.^[30] This similarity is also expected and we only discuss the energetic changes, and the structural parameters are given for comparison. The CO addition to propenyl complex **A2B** or **P2L** giving **A3B** or **P3L** does not have any barrier and is exergonic by 6.3 or 8.2 kcal mol $^{-1}$ (Figures 7 and 9, top). It is also noteworthy that **A3L** is still more stable than **A3B** by 1.2 kcal mol $^{-1}$, but the energy difference decreases considerably relative to 16.3 kcal mol $^{-1}$ between **A2L** and **A2B**.

The successive carbonylation of **A3B** or **P3L** performs by two steps. First, the propenyl group migrates to a *cis* carbonyl coupled with the skeletal change leading to the η^3 -acyl complex (**A4Ba** or **P4La**). Second, **A4Ba** or **P4La** transforms to the η^2 -acyl complex (**A4Bb** or **P4Lb**) with acyl group at the axial site and η^2 -O=C stabilization at equatorial site. As illustrated in Figures 7 and 9 (top), for both reaction paths AB and PL, these two steps have moderate free energy barriers of 6.5/7.0 and 11.2/9.5 kcal mol $^{-1}$. In addition, for path AB, the first step is exergonic by 3.8 kcal mol $^{-1}$, and the second step is endergonic by 2.3 kcal mol $^{-1}$, while two steps for path PL are nearly thermal neutral processes (–0.8 and –0.3 kcal mol $^{-1}$).

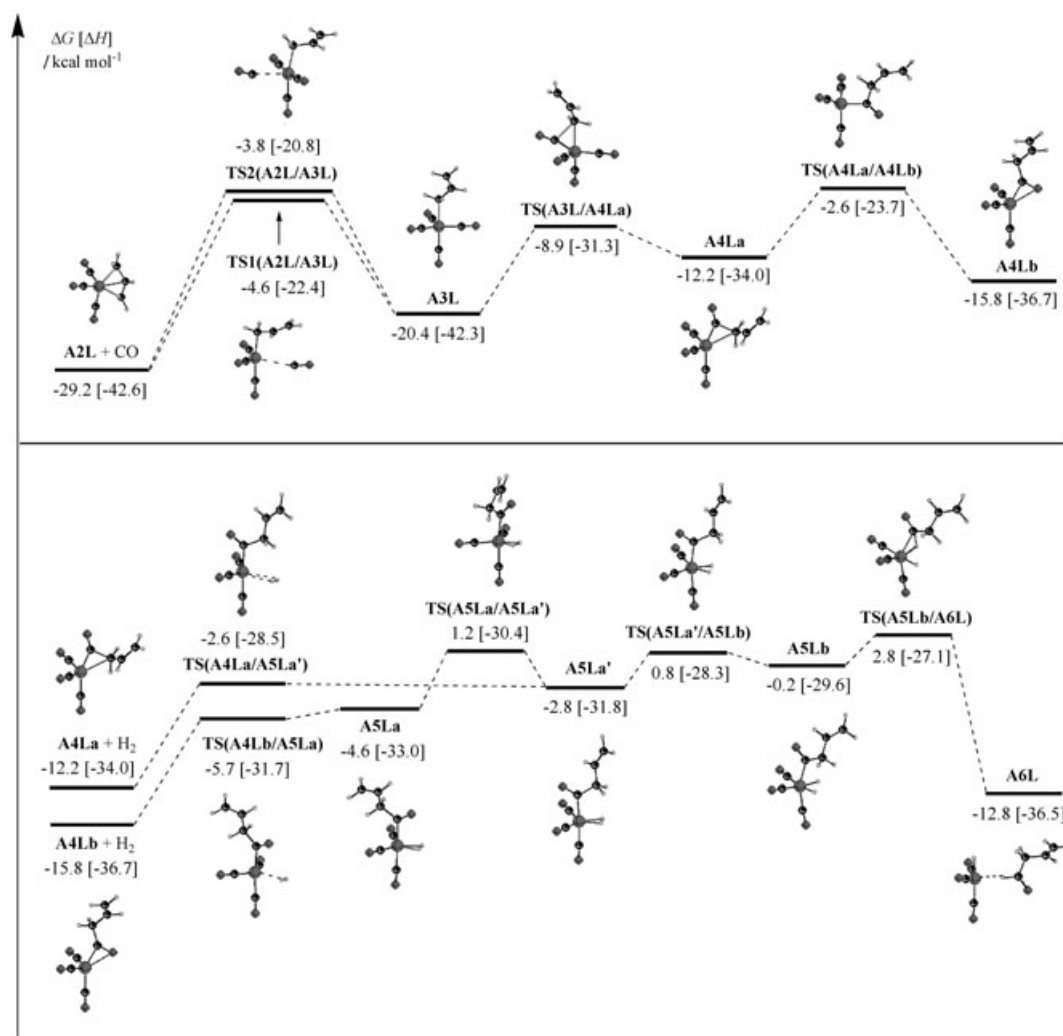


Figure 5. Free energy profiles (kcal mol^{-1} , enthalpies in square brackets) for CO addition and insertion (relative to $[\text{HCo}(\text{CO})_3] + \text{allene} + \text{CO}$, top) and for H_2 oxidative addition and unsaturated aldehyde elimination of path AL (relative to $[\text{HCo}(\text{CO})_3] + \text{allene} + \text{CO} + \text{H}_2$, bottom).

After that, H_2 coordination to η^2 -acyl complex (**A4Bb** or **P4Lb**) forming the hydrogen complex (**A5Ba** or **P5La**) occurs without additional free energy barrier, and is endergonic by 13.5 or 13.6 kcal mol^{-1} . The following H_2 oxidative addition (**A5Ba** \rightarrow **A5Bb** or **P5La** \rightarrow **P5Lb**) is a one-step process, and is also endergonic by 9.3 or 9.6 kcal mol^{-1} (Figures 7 and 9, bottom). Finally, the elimination of unsaturated aldehyde from dihydride complex **A5Bb** or **P5Lb** proceeds via the three-center transition state leading to the adduct **A6B** or **P6L**. This step is predicted to be a rapid and highly exergonic process (-21.2 or -20.6 kcal mol^{-1}).

Catalytic isomerization of propyne and allene: The thermal isomerization of propyne and allene takes place at elevated temperature, and this reaction has been well studied both experimentally and theoretically.^[36–42] Several mechanisms have been proposed, and the most popular one is the step-wise process involving the formation of cyclopropene intermediate.^[37,41] The kinetic experiments and the theoretical

calculations further revealed that this thermal process has a barrier about 65 kcal mol^{-1} .^[38,41]

Apart from the thermal process, the catalytic isomerization of propyne and allene can be mediated by transition-metal complexes.^[43] In this case, a mechanism involving the cyclopropene intermediate is not operative. According to the results discussed above (Figures 1 and 3), two possible pathways can be thought for the catalytic isomerization, that is, i) isomerization via the joint Markovnikov intermediate **A2B** and ii) isomerization via the anti-Markovnikov intermediates **P2L** and **A2L**.

Isomerization via the Markovnikov intermediate (A2B):

Combining the results of propyne and allene hydroformylation, the free energy profiles for the catalytic isomerization of propyne and allene via **A2B** is depicted in Figure 11. For the process of propyne to allene, the reaction **A2B'** \rightarrow **A1** has the highest free energy barrier of 19.9 kcal mol^{-1} , while for the reverse process of allene to propyne, the reaction

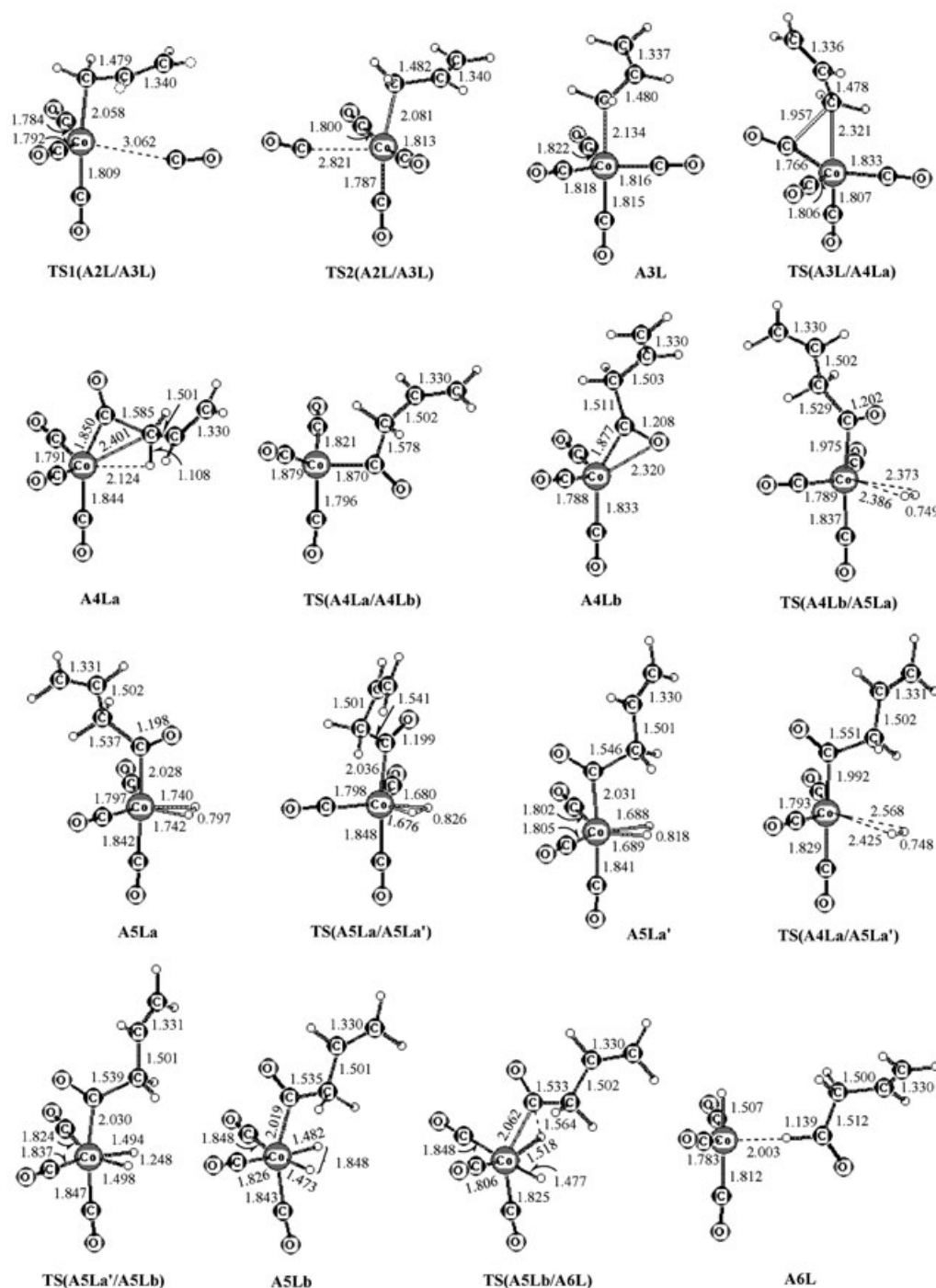


Figure 6. Bond lengths [Å] of the stationary points involved in CO addition and insertion, H₂ oxidative addition and unsaturated aldehyde elimination of path AL.

A2B → **P1** has the highest free energy barrier of 23.1 kcal mol⁻¹. On the basis of this energetic difference and the relative stability between **A1** and **P1** (3.1 kcal mol⁻¹ in free energy), the isomerization from propyne to allene should be more favored.

Isomerization via the anti-Markovnikov intermediates (P2L and A2L): The essential of the interconversion be-

tween propyne and allene is accomplishing a 1,3-H shift.^[36] Considered as a substituted olefin, **P2L** has a *trans* configuration. In this form, a direct transfer of the methyl hydrogen to cobalt is not possible. Therefore, the intermediate **P2L** should first convert to the *cis* form **5**, and then the formal 1,3-H shift occurs (**5** → **A2L**). The free energy profiles for this process are displayed in Figure 12, while the structures of the stationary points are illustrated in Figure 13.

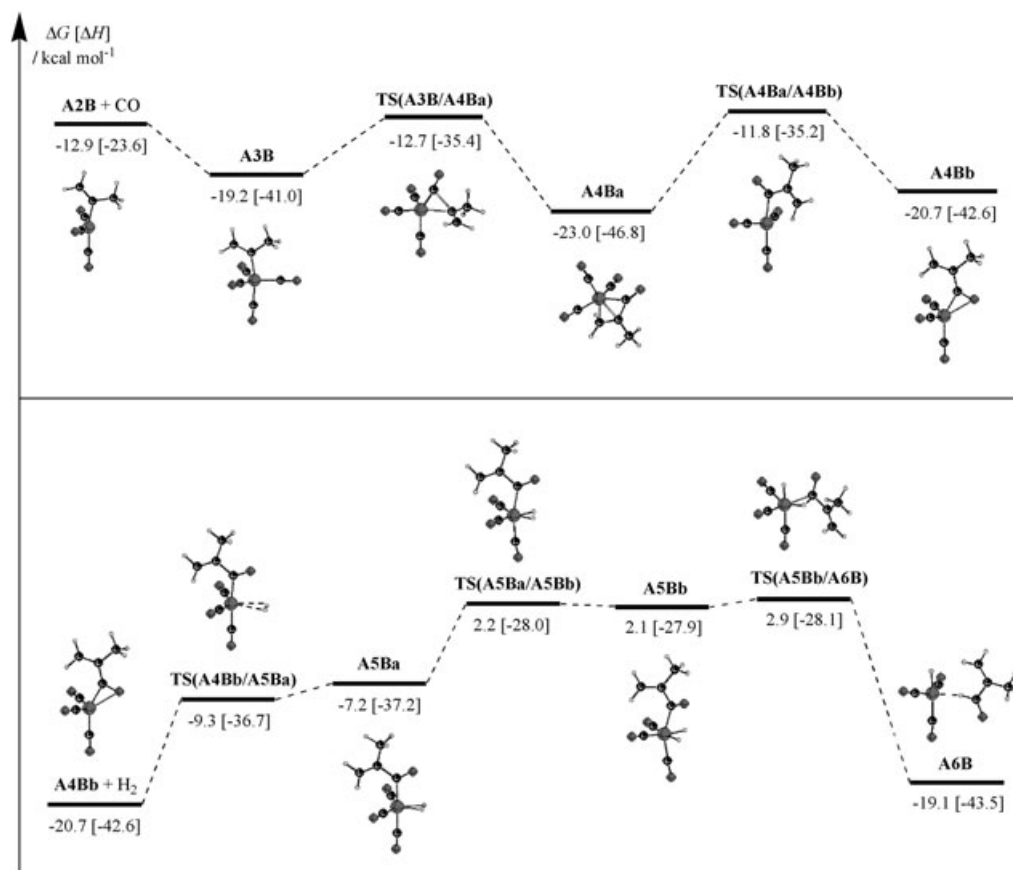


Figure 7. Free energy profiles (kcal mol⁻¹, enthalpies in square brackets) for CO addition and insertion (relative to [HCo(CO)₃] + allene + CO, top) and for H₂ oxidative addition and unsaturated aldehyde elimination of path AB (relative to [HCo(CO)₃] + allene + CO + H₂, bottom).

In the course of **P2L** to **A2L**, the interconversion of the *trans* and *cis* configurations of the propenyl complex [(H₃CHC=CH)Co(CO)₃], **P2L** and **5**, is the key process. It proceeds by three steps: a) the α -H transfer from carbon atom (-CHCHCH₃) to cobalt, b) the vinylidene moiety (C=CHCH₃) rotation, and c) the hydride transfer from cobalt to α carbon atom.

Starting from **P2L**, the α -H transfer to cobalt results in the trigonal bipyramidal complex **3**, in which the C=CHCH₃ group and the hydride occupy the axial sites. In particular, the β -H of the C=CHCH₃ group is eclipsed with one of the equatorial carbonyl ligands. In the corresponding transition state **TS(P2L/3)**, the hydrogen atom shifts to cobalt, while at the equatorial site. The imaginary vibration mode indicates that the late process of **TS(P2L/3)** \rightarrow **3** goes by the simultaneous rotation of the hydride and the axial CO. As shown in Figure 12, this step (**P2L** \rightarrow **3**) is endergonic by 23.9 kcal mol⁻¹ with a high free energy barrier of 35.9 kcal mol⁻¹.

The rotation of the vinylidene group (C=CHCH₃) is the subsequent step, which is a rapid process with a low free energy barrier of 2.0 kcal mol⁻¹. Relative to complex **3**, the C=CHCH₃ moiety rotates about 35° in the corresponding transition state **TS(3/4)** and 67° in complex **4**. In complex **4**,

the methyl group is eclipsed with one of the equatorial carbonyl ligands.

Next, the hydride transfer to the 2-carbon atom goes via the transition state **TS(4/5)** leading to the *cis* species **5**. This step (**4** \rightarrow **5**) is predicted to be exergonic by 24.2 kcal mol⁻¹, and has a moderate free energy barrier of 11.9 kcal mol⁻¹. As shown in Figure 12, both the *trans*- and *cis*-propenyl complexes (**P2L** and **5**) are nearly equal in energy, and two vinylidene complexes (**3** and **4**) are also approximately equal in energy. The most interesting point is that the total barrier for the formal C=C double-bond rotation via this stepwise process is about 36 kcal mol⁻¹, which is much smaller than the thermal process of ethylene (64 kcal mol⁻¹)^[44] and fluorine substituted olefins (52–65 kcal mol⁻¹).^[45]

In the following section, we will pay attention to the formal 1,3-H shift. As depicted in Figure 12, the formal 1,3-H shift (**5** \rightarrow **A2L**) is a stepwise process. It involves two elementary steps, that is, a) the hydrogen atom transfer from methyl to cobalt with the formation of complex **6**, and b) the hydride transfer from cobalt to the terminal carbon atom (=CH) of the CH=CHCH₂ group with the formation of allylic complex **A2L**.

Starting with **5**, the hydrogen atom of methyl transfer to cobalt proceeds via the transition state **TS(5/6)** leading to

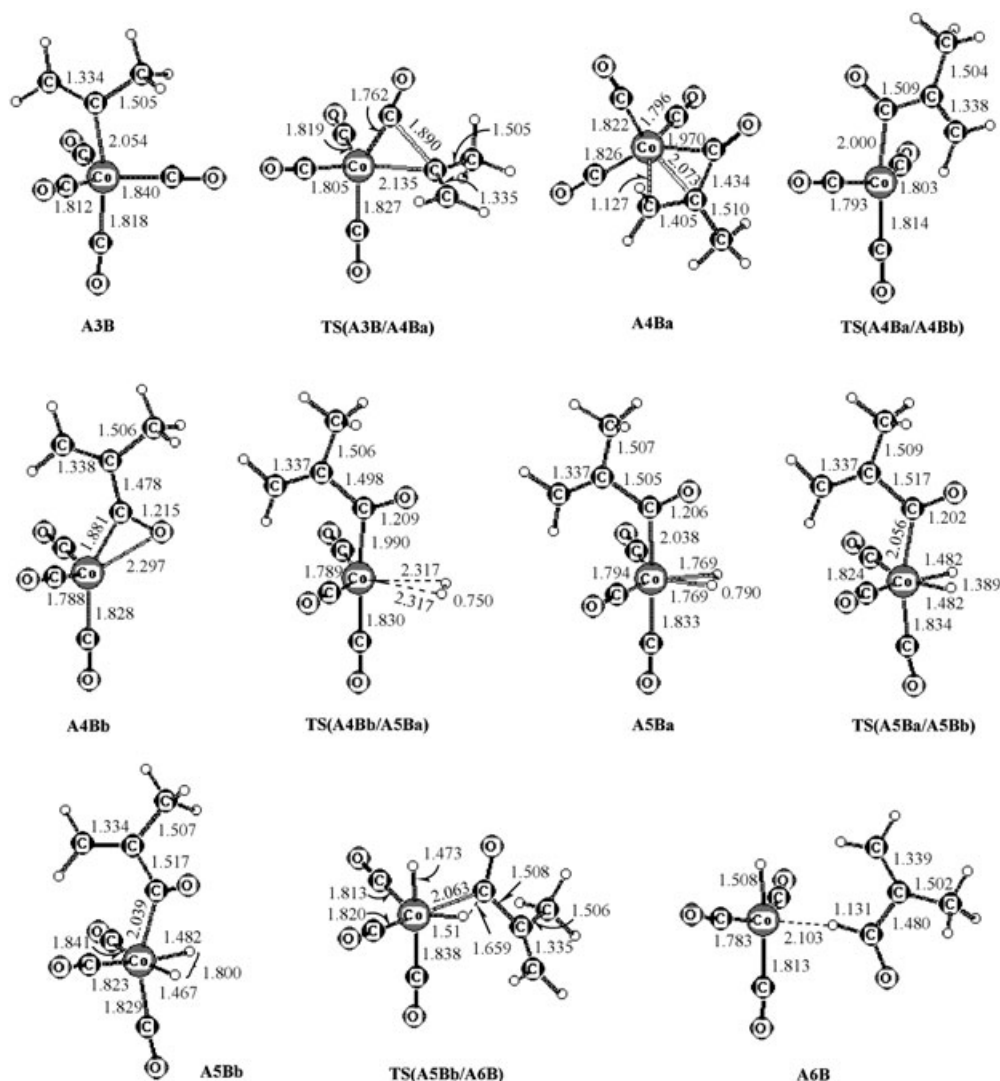


Figure 8. Bond lengths [Å] of the stationary points involved in CO addition and insertion, H₂ oxidative addition and unsaturated aldehyde elimination of path AB.

the η^2 intermediate **6**. As shown in Figure 13, the η^2 intermediate **6** has a trigonal bipyramidal geometry, in which the CH=CHCH₂ group attaches to [HCo(CO)₃] moiety through the 1,3-carbon atoms forming a four-membered ring. Moreover, the corresponding transition state TS(**5/6**) is structurally similar to the intermediate **6**, and is a late transition state. From the free energy profiles in Figure 12, it is evident that the η^2 intermediate **6** is higher in free energy than the propenyl complex **5** by 36.3 kcal mol⁻¹, and the related hydrogen-transfer reaction (**5** → TS(**5/6**) → **6**) can be accomplished by overcoming a high free energy barrier of 41.0 kcal mol⁻¹.

Due to the low stability, the η^2 intermediate **6** easily proceeds the hydrogen-transfer reaction via TS(**6/A2L**) leading to the more stable allylic complex **A2L**. The hydride transfer from cobalt to the terminal carbon atom (=CH) of the CH=CHCH₂ group is highly exergonic by 51.8 kcal mol⁻¹, and has a very low free energy barrier of 0.9 kcal mol⁻¹.

For the isomerization of propyne to allene (Figure 12), the highest free energy barrier is associated with the reaction **5** → **6** (41.0 kcal mol⁻¹), while that for the reverse process is related to the reaction **A2L** → **6** (52.7 kcal mol⁻¹). On the bases of this energetic difference and the relative stability between **A2L** and **P2L** (15.6 kcal mol⁻¹), the conversion from propyne to allene is more likely.

At this stage, one might ask the most likely reaction path for the interconversion of propyne and allene. As shown in Figures 11 and 12, the conversion from **A2B** to **A1** has lower barrier than that from **P2L** to **A1**, and this indicates that the process from **A2B** to **A1** should be more favored. On the other hand, the barriers for the reverse process of propyne insertion reactions (**P2L** and **A2B** to **P1**; 24.0 and 23.1 kcal mol⁻¹) are lower than that (35.9 kcal mol⁻¹) for the isomerization of *trans* to *cis* propenyl complexes (**P2L** → **5**). This indicates that the former one is more favored, and the latter one is not competitive. On the basis of these ener-

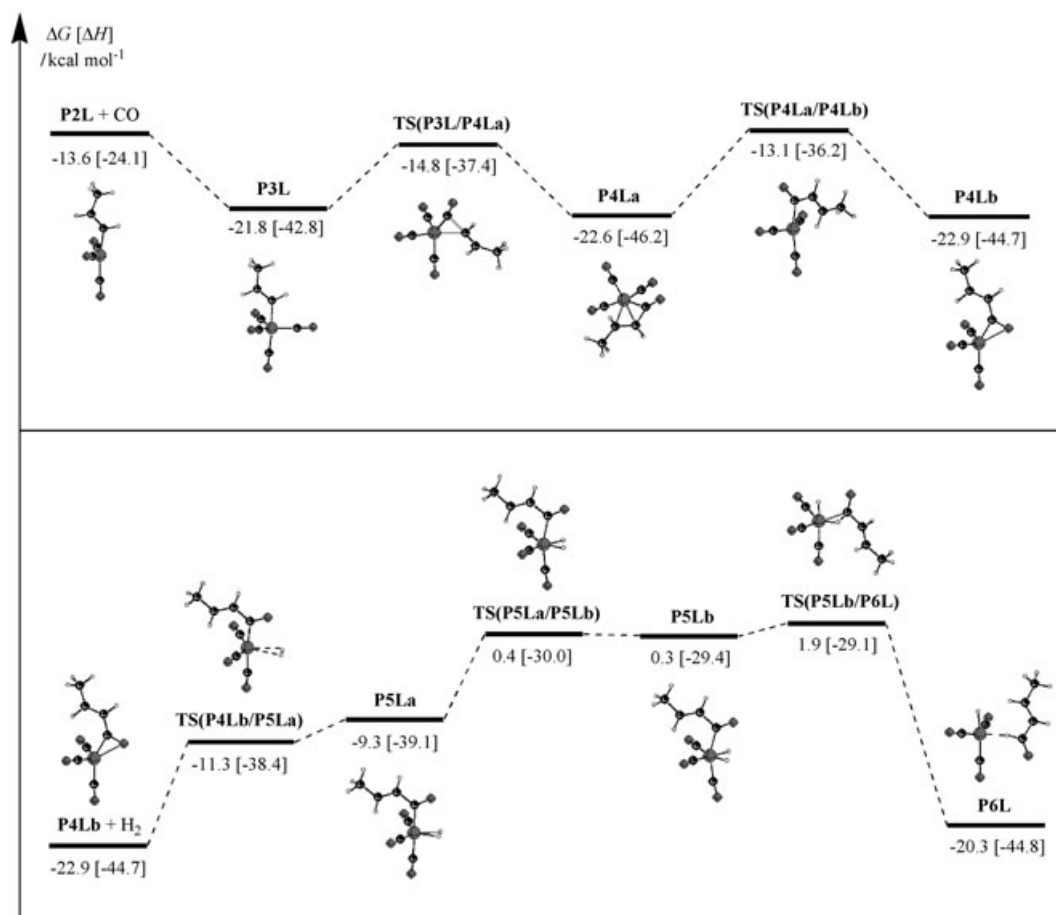


Figure 9. Free energy profiles (kcal mol⁻¹, enthalpies in square brackets) for CO addition and insertion (relative to [HCo(CO)₃] + allene + CO, top) and for H₂ oxidative addition and unsaturated aldehyde elimination of path PL (relative to [HCo(CO)₃] + allene + CO + H₂, bottom).

getic data, it is reasonable to consider the most likely conversion path from propyne to allene as **P2L** → **P1** → **A2B** → **A1**. In contrast, the process from allene to propyne with the highest barrier (**A2L** to **6**, 52.7 kcal mol⁻¹) is less likely.

Regioselectivity: As a potential competitive reaction, the catalytic isomerization is likely to change the product composition and distribution of the allene and propyne hydroformylation. The corresponding Gibbs free energies of activation (ΔG^\ddagger) and reaction (ΔG) are collected in Table 1. These results clearly show that the CO addition reactions have lower Gibbs free energies of activation and reaction than the corresponding isomerization steps, and the energetic differences are larger than 18.9 kcal mol⁻¹. Therefore, the isomerization is not competitive to the CO addition both kinetically and thermodynamically. Under the hydroformylation reaction conditions, the catalytic isomerization cannot occur.

The hydroformylation of allene gives the anti-Markovnikov product H₂C=CHCH₂CHO and the Markovnikov product H₂C=C(CH₃)CHO, while that of propyne forms the different anti-Markovnikov product H₃CHC=CHCHO and the mutual Markovnikov product H₂C=C(CH₃)CHO. In both

Table 1. Gibbs free energies [kcal mol⁻¹] of activation (ΔG^\ddagger) and reaction (ΔG).

Reaction	ΔG^\ddagger	ΔG
CO addition		
P2L + CO → TS(P2L/P3L) → P3L	0.0	-8.2
A2B + CO → TS(A2B/A3B) → A3B	0.0	-6.3
A2L + CO → TS1(A2L/A3L) → A3L	24.6	8.8
<i>trans-cis</i> isomerization		
P2L → TS(P2L/3) → 3	35.9	23.9
reverse reaction of allene insertion		
A2B ↔ A2B' → TS(A1/A2B') → A1	20.6	12.6
reverse reaction of propyne insertion		
A2B → TS(P1/A2B) → P1	23.1	15.7
1,3-H shift		
A2L → TS(6/A2L) → 6	52.7	51.8

cases, the regioselectivity (anti-M:M) is determined by the irreversible reaction step of allene or propyne insertion into the Co-H bond. As depicted in Figure 1, the allene hydroformylation presents a kinetic and thermodynamic preference for anti-Markovnikov insertion, for example **TS(A1/A2L)** is lower in free energy than **TS(A1/A2B')** by 3.2 kcal mol⁻¹, and the anti-Markovnikov intermediate **A2L** is more favored energetically than the Markovnikov inter-

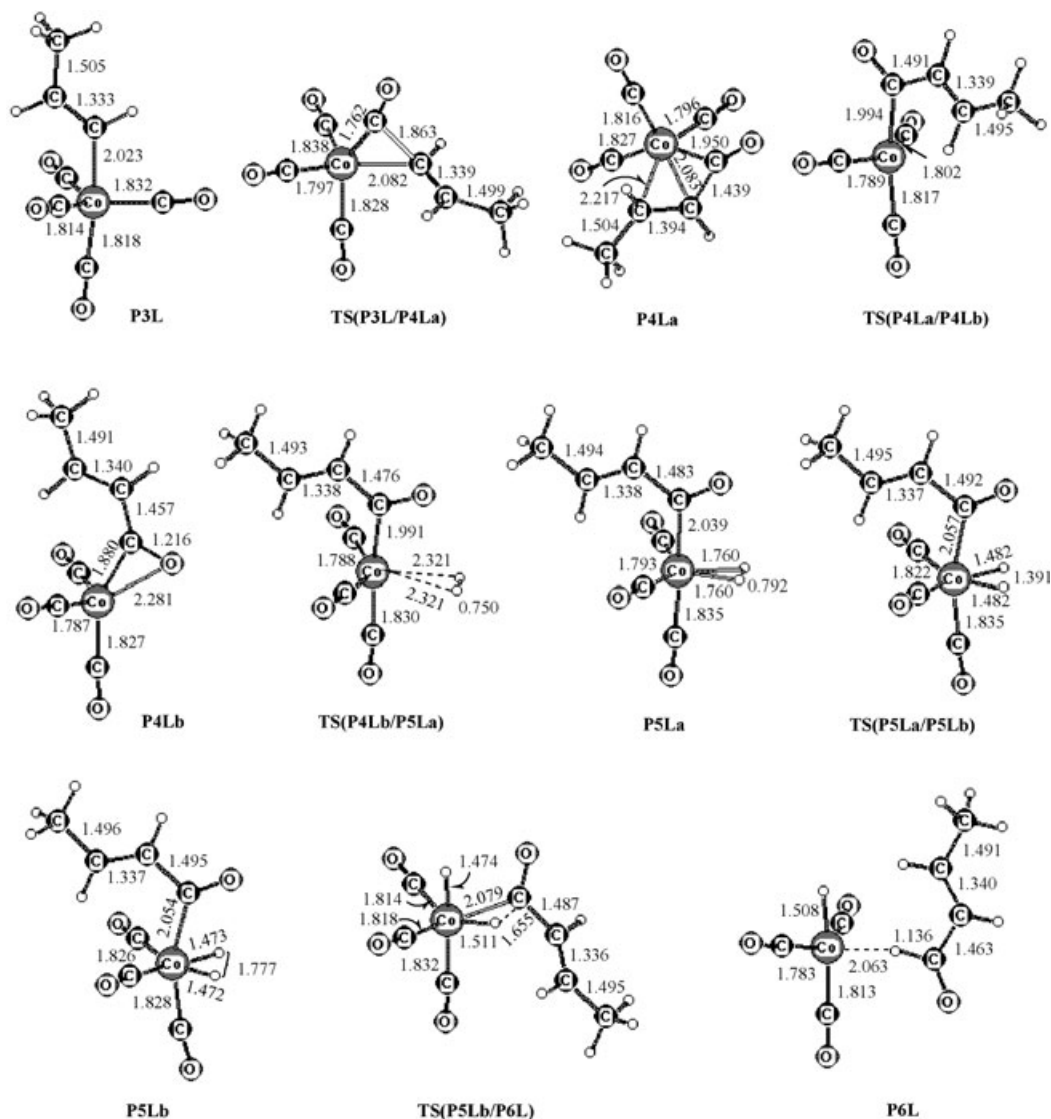


Figure 10. Bond lengths [Å] of the stationary points involved in CO addition and insertion, H_2 oxidative addition and unsaturated aldehyde elimination of path PL.

mediate **A2B** by $16.3 \text{ kcal mol}^{-1}$. In terms of these energy differences, a percentage ratio of 98:2 for anti-Markovnikov to Markovnikov products is predicted kinetically. Furthermore, from the thermodynamic point of view, the predicted product ratio would be quantitative. Therefore, the linear unsaturated aldehyde should be the principal product (but it is to note that the terminal $\text{C}=\text{C}$ bond can be used for second cycle reaction to form dialdehyde as found experimentally^[28]). As being much more stable than the allene and propenyl complexes (**A1** and **A2B**) by -28.9 and $-16.3 \text{ kcal mol}^{-1}$, the allyl complex **A2L** should exist in stable form. In addition, the free energy barrier of CO addition to **A2L** by $24.6 \text{ kcal mol}^{-1}$ indicates the enhanced kinetic stability. Therefore, **A2L** could be isolated as stable intermediate under the exclusion of CO. It is to note that **A2L** can further react with CO/H_2 to yield the same product as allene hydroformylation under the actual reaction conditions.

However, the propyne hydroformylation is considerably different. From the kinetic point of view, **TS(P1/P2L)** is $0.2 \text{ kcal mol}^{-1}$ higher in free energy than **TS(P1/A2B)**, and no regioselectivity can be expected. On the other hand, the intermediate **P2L** is more stable than **A2B** by $0.7 \text{ kcal mol}^{-1}$, and this energy difference favors the anti-Markovnikov over Markovnikov products (70:30). From the kinetic and thermodynamic aspects, propyne hydroformylation would be not regioselective.

It is noteworthy that if carbon monoxide is not present, the $[\text{HCo}(\text{CO})_3]$ -catalyzed isomerization of propyne to allene can take place. This property provides an opportunity for the optimization or manipulation of reaction conditions, such as the sequence and addition time, to get the desired product distribution.

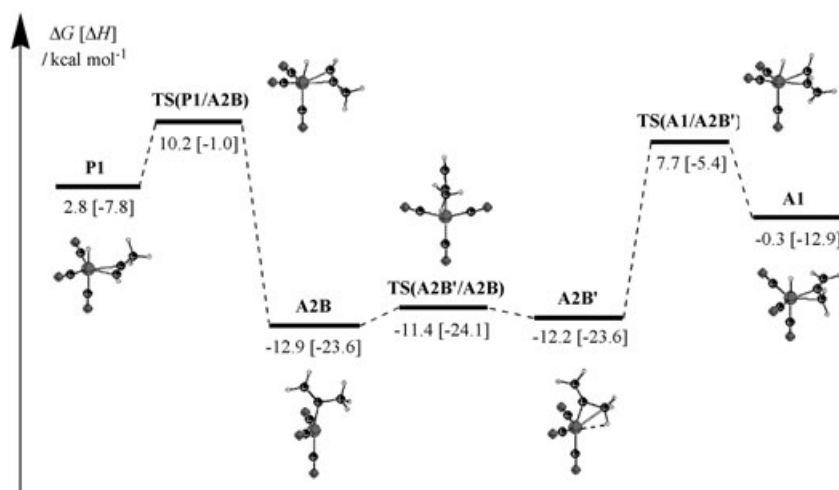


Figure 11. Free energy profiles (kcal mol^{-1} , enthalpies in square brackets) for isomerization via the Markovnikov intermediate (relative to $[\text{HCo}(\text{CO})_3] + \text{allene}$).

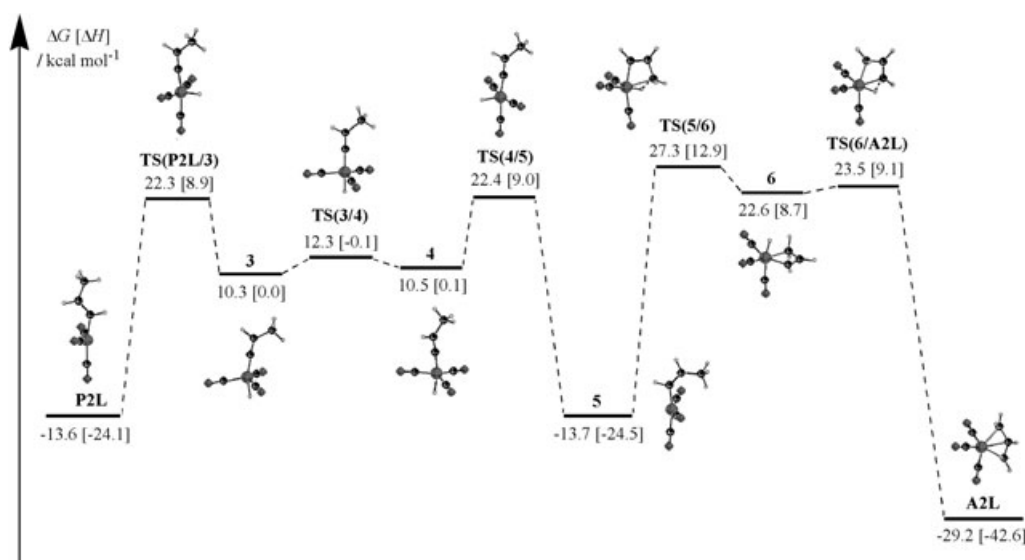


Figure 12. Free energy profiles (kcal mol^{-1} , enthalpies in square brackets) for isomerization via the anti-Markovnikov intermediates (relative to $[\text{HCo}(\text{CO})_3] + \text{allene}$).

Conclusion

In this paper, we have presented a comprehensive computational study on the $[\text{HCo}(\text{CO})_3]$ -catalyzed hydroformylation of allene and propyne employing the B3LYP density functional method.

For allene hydroformylation, it is found that allene insertion step is an irreversible process, and is in control of the regioselectivity. Both kinetic and thermodynamic effects favor the linear anti-Markovnikov intermediate **A2L** $[(\eta^3\text{-CH}_2\text{CHCH}_2)\text{Co}(\text{CO})_3]$, and the formation of the branched Markovnikov intermediate **A2B** $[(\text{H}_2\text{C}=\text{CCH}_3)\text{Co}(\text{CO})_3]$ is not competitive. As a consequence, the linear aldehyde

would be the predominant product. By contrast, propyne hydroformylation is computed to be not regioselective, since the formation of the linear anti-Markovnikov **P2L** $[(\text{CH}_3\text{CH}=\text{CH})\text{Co}(\text{CO})_3]$ and branched Markovnikov **A2B** intermediates has equal probability.

In addition to hydroformylation, the possible paths of isomerization between propyne and allene with $[\text{HCo}(\text{CO})_3]$ via anti-Markovnikov and Markovnikov intermediates have been investigated. On the basis of the computed energetic data, the conversion from propyne to allene should be more likely, while that from allene to propyne should be less likely.

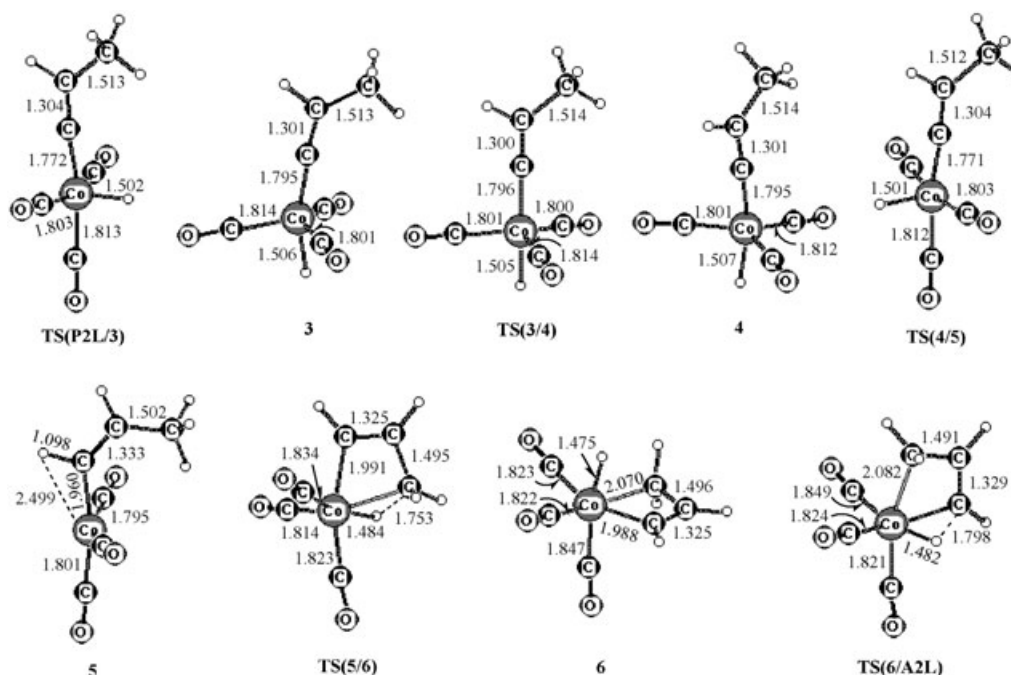


Figure 13. Bond lengths [Å] of the stationary points involved in isomerization via the anti-Markovnikov intermediates.

Acknowledgement

This work was supported by Chinese Academy of Sciences (20029908) and the National Natural Science Foundation China.

- [1] a) P. W. N. M. van Leeuwen, C. Claver, *Rhodium Catalyzed Hydroformylation*, Kluwer Academic Publishers, Dordrecht, Netherlands, **2000**; b) J. Falbe, *New Syntheses with Carbon Monoxide*, Springer, Berlin, **1980**; c) M. Torrent, M. Solà, G. Frenking, *Chem. Rev.* **2000**, *100*, 439–493.
- [2] M. Beller, B. Cornils, C. D. Frohning, C. W. Kohlpaintner, *J. Mol. Catal. A* **1995**, *104*, 17–85.
- [3] G. W. Parshall, S. D. Ittel, *Homogeneous Catalysis*, Wiley, New York, **1992**.
- [4] B. Cornils, W. A. Herrmann, *Applied Homogeneous Catalysis with Organometallic Compounds*, Vol. 1, Wiley-VCH, Weinheim, **2002**.
- [5] M. Orchin, W. Rupilius, *Catal. Rev.* **1972**, *6*, 85–131.
- [6] G. Süß-Fink, G. Meister, *Adv. Organomet. Chem.* **1993**, *35*, 41–134.
- [7] G. Papadogianakis, R. A. Sheldon, *New J. Chem.* **1996**, *20*, 175–185.
- [8] B. Cornils, L. Markó in *Methoden der organischen Chemie (Houben-Weyl)*, Vol. E18, 4th ed., Thieme, Stuttgart, New York, **1986**.
- [9] G. Natta, P. Pino, *The 12th International Congress of Pure and Applied Chemistry*, New York, September **1951**.
- [10] H. Greenfield, J. H. Wotiz, I. Wender, *J. Org. Chem.* **1957**, *22*, 542–546.
- [11] B. Fell, M. Beutler, *Tetrahedron Lett.* **1972**, *13*, 3455–3456.
- [12] C. Botteghi, Ch. Salomon, *Tetrahedron Lett.* **1974**, *15*, 4285–4288.
- [13] K. Doyama, T. Joh, T. Shiohara, S. Takahashi, *Bull. Chem. Soc. Jpn.* **1988**, *61*, 4353–4360.
- [14] P. G. M. Wuts, A. R. Ritter, *J. Org. Chem.* **1989**, *54*, 5180–5182.
- [15] E. M. Campi, W. R. Jackson, Y. Nilsson, *Tetrahedron Lett.* **1991**, *32*, 1093–1094.
- [16] P. Nombel, N. Lugan, F. Mulla, G. Lavigne, *Organometallics* **1994**, *13*, 4673–4675.
- [17] J. R. Johnson, G. D. Cuny, S. L. Buchwald, *Angew. Chem.* **1995**, *107*, 1877–1878; *Angew. Chem. Int. Ed. Engl.* **1995**, *34*, 1760–1761.
- [18] Y. Ishii, K. Miyashita, K. Kamita, M. Hidai, *J. Am. Chem. Soc.* **1997**, *119*, 6448–6449.
- [19] B. G. Van den Hoven, H. Alper, *J. Org. Chem.* **1999**, *64*, 3964–3968.
- [20] B. G. Van den Hoven, H. Alper, *J. Org. Chem.* **1999**, *64*, 9640–9645.
- [21] R. Zimmer, C. U. Dinesh, E. Nandanan, F. A. Khan, *Chem. Rev.* **2000**, *100*, 3067–3125.
- [22] F.-Y. Yang, M.-Y. Wu, C.-H. Cheng, *J. Am. Chem. Soc.* **2000**, *122*, 7122–7123.
- [23] S. Saito, K. Hirayama, C. Kabuto, Y. Yamamoto, *J. Am. Chem. Soc.* **2000**, *122*, 10776–10780.
- [24] B. M. Trost, C. Jäkel, B. Plietker, *J. Am. Chem. Soc.* **2003**, *125*, 4438–4439.
- [25] T. J. Kealy, R. E. Benson, *J. Org. Chem.* **1961**, *26*, 3126–3130.
- [26] L. Ackermann, R. G. Bergman, R. N. Loy, *J. Am. Chem. Soc.* **2003**, *125*, 11956–11963.
- [27] L. Canovese, F. Visentin, G. Chessa, P. Uguagliati, G. Bandoli, *Organometallics* **2000**, *19*, 1461–1463.
- [28] B. Fell, M. Beutler, *Erdöl und Kohle, Erdgas*, **1976**, *29*, 149–153.
- [29] For a recent review on transition metal catalyzed regioselective functionalization of alkenes and alkynes, see: M. Beller, J. Seayad, A. Tillack, H. Jiao, *Angew. Chem.* **2004**, *116*, 3448–3479; *Angew. Chem. Int. Ed.* **2004**, *43*, 3368–3398.
- [30] C.-F. Huo, Y.-W. Li, M. Beller, H. Jiao, *Organometallics* **2004**, *23*, 765–773.
- [31] R. F. Heck, D. S. Breslow, *J. Am. Chem. Soc.* **1961**, *83*, 4023–4027.
- [32] Gaussian 03, M. J. Frisch, G. W. Trucks, H. B. Schlegel, G. E. Scuseria, M. A. Robb, J. R. Cheeseman, J. A. Montgomery, Jr., T. Vreven, K. N. Kudin, J. C. Burant, J. M. Millam, S. S. Iyengar, J. Tomasi, V. Barone, B. Mennucci, M. Cossi, G. Scalmani, N. Rega, G. A. Petersson, H. Nakatsuji, M. Hada, M. Ehara, K. Toyota, R. Fukuda, J. Hasegawa, M. Ishida, T. Nakajima, Y. Honda, O. Kitao, H. Nakai, M. Klene, X. Li, J. E. Knox, H. P. Hratchian, J. B. Cross, C. Adamo, J. Jaramillo, R. Gomperts, R. E. Stratmann, O. Yazyev, A. J. Austin, R. Cammi, C. Pomelli, J. W. Ochterski, P. Y. Ayala, K. Morokuma, G. A. Voth, P. Salvador, J. J. Dannenberg, V. G. Zakrzewski, S. Dapprich, A. D. Daniels, M. C. Strain, O. Farkas, D. K. Malick, A. D. Rabuck, K. Raghavachari, J. B. Foresman, J. V. Ortiz, Q. Cui, A. G.

- Baboul, S. Clifford, J. Cioslowski, B. B. Stefanov, G. Liu, A. Liashenko, P. Piskorz, I. Komaromi, R. L. Martin, D. J. Fox, T. Keith, M. A. Al-Laham, C. Y. Peng, A. Nanayakkara, M. Challacombe, P. M. W. Gill, B. Johnson, W. Chen, M. W. Wong, C. Gonzalez, J. A. Pople, Gaussian Inc., Pittsburgh PA, **2003**.
- [33] J. W. Ochterski, *Thermochemistry in Gaussian* (see: help@Gaussian.com).
- [34] C.-F. Huo, Y.-W. Li, M. Beller, H. Jiao, *Organometallics* **2003**, *22*, 4665–4677.
- [35] C.-F. Huo, Y.-W. Li, G.-S. Wu, M. Beller, H. Jiao, *J. Phys. Chem. A* **2002**, *106*, 12161–12169.
- [36] A. Lifshitz, M. Frenklach, A. Burcat, *J. Phys. Chem.* **1975**, *79*, 1148–1152.
- [37] H. Hopf, H. Priebe, R. Walsh, *J. Am. Chem. Soc.* **1980**, *102*, 1210–1212.
- [38] M. Karni, I. Oref, S. Barzilai-Gilboa, A. Lifshitz, *J. Phys. Chem.* **1988**, *92*, 6924–6929.
- [39] T. Kakumoto, T. Ushirogouchi, K. Saito, A. Imamura, *J. Phys. Chem.* **1987**, *91*, 183–189.
- [40] a) N. Honjou, J. Pacansky, M. Yoshimine, *J. Am. Chem. Soc.* **1984**, *106*, 5361–5363; b) N. Honjou, J. Pacansky, M. Yoshimine, *J. Am. Chem. Soc.* **1985**, *107*, 5332–5341.
- [41] a) M. Yoshimine, J. Pacansky, N. Honjou, *J. Am. Chem. Soc.* **1989**, *111*, 2785–2798; b) M. Yoshimine, J. Pacansky, N. Honjou, *J. Am. Chem. Soc.* **1989**, *111*, 4198–4209.
- [42] J. H. Kiefer, P. S. Mudipalli, S. S. Sidhu, R. D. Kern, B. S. Jursic, K. Xie, H. Chen, *J. Phys. Chem. A* **1997**, *101*, 4057–4071.
- [43] A. Salvini, F. Piacenti, P. Frediani, A. Devescovi, M. Caporali, *J. Organomet. Chem.* **2001**, *625*, 255–267.
- [44] J. E. Douglas, B. S. Rabinovitch, F. S. Looney, *J. Chem. Phys.* **1955**, *23*, 315–323.
- [45] Y. L. Wang, R. A. Poirier, *Can. J. Chem.* **1998**, *76*, 477–482.

Received: July 15, 2004
Published online: December 9, 2004